IOSR Journal of Mechanical and Civil Engineering (IOSR-JMCE)
e-ISSN: 2278-1684,p-ISSN: 2320-334X, Volume 21, Issue 1 Ser. 2 (Jan. – Feb. 2024), PP 01-08
www.iosrjournals.org

Comparison Of The Flexural Capacity Of Beams With Web Openings And Solid I-Beams

Serkan Taş[1]
[1](*Department Of Civil Engineering / Akdeniz University, Turkey)*

Abstract:
The aim of the research is to experimentally present the load-carrying capacities and failure modes of web expanded steel cellular beams and solid I-beams under the same load conditions. The experiments were conducted at full scale on non-composite beams. In this study, two tests were performed for web expanded cellular beams, and one test was conducted for solid I-beam, using IPE200 coded profiles. The spans of the beams were selected as 5.5 meters, and a point load was applied at the center of the upper flange. The design methods for the beams were based on the provisions of BS 5950.

Key Word*: Cellular beams; Solid I-beams; Web-expanded beams; Steel structures; Load capacity*

Date of Submission: 07-01-2024 Date of Acceptance: 17-01-2024

I. Introduction

In building systems, large spans that cannot be spanned by reinforced concrete structural members can be effectively spanned thanks to the flexibility of steel structural systems. Particularly, steel beams with web openings, featuring advanced designs that provide greater flexibility compared to other beams, stand out. The primary objective in the production of these beams is to increase the existing beam height and, consequently, the moment of inertia. The increase in moment of inertia enhances the beam's strength and rigidity, resulting in a more robust structure. Due to the advantages of weight and cost savings, these steel beams offer an effective solution, especially in large-span areas where intermediate columns are undesirable, such as shopping centers, sports facilities, office buildings, and parking lots. These steel beams play a significant role in both technical and economic aspects of modern structural designs.

Beams with increased depth were initially considered by structural engineers during World War II, primarily with the aim of reducing the cost of steel structures, especially in castellated beam applications. The rigidity and moment of inertia increase achieved without the need for material reinforcement in I-section profile beams marked a turning point in steel structure designs. The significance of these beams in the literature began with Altifillisch et al. (1957)'s[1] study, which examined the plastic and elastic behaviors under singular loading. Husain and Speirs (1971)[2] conducted various tests under different loading conditions to examine yielding and fractures in the welding zones of steel castellated beams. Sherbourne (1966)[3] experimental program designed for various castellated beam specimens investigated the interaction between moment and shear force in steel castellated beams, marking a significant contribution to the field. One of the fundamental challenges faced by beams with increased depth is the lateral buckling, especially in long spans and inadequate lateral support conditions, occurring at the upper flange of the beam. This phenomenon, identified by Kerdal and Nethercot (1982)[4], is attributed to the deeper and more slender cross-section of the beam compared to its initial state, particularly leading to the occurrence of such lateral deflection situations. Castellated beams, despite being a structure type that has been studied with traditional and modern methods in the literature, have limited theoretical and experimental publications on cellular beams. These beams were utilized in full-scale tests by Lawson (1988)[5] to verify the structural integrity and design criteria of the beams. In the experiments, it was observed that the beams yielded to lateral buckling under the applied load. The design of simple cellular beams according to the BS (British Standard) 5950 specification was presented by Ward (1990)[6]. The bending, local, and overall strength modes derived from a parametric study of these beams were supported by a detailed finite element analysis. The most comprehensive recent study on cellular beams was conducted by Hoffman et al. (2012)[7]. In these studies, stress distributions around the web openings were examined.

Within the scope of this study, cellular steel beams and their original forms were experimentally examined. During the experiments, the load-carrying capacities, behavioral characteristics, and failure modes of these beams were compared.

II. Material And Methods

Web-expanded beams; they are formed by cutting the lower and upper parts obtained by CNC (Computer Numerical Control) method in the shape of a half-circle, sawtooth, or sine curve, depending on the geometry along the web of the steel I-section profile, and then sliding and rejoining them by welding. As a result of the processes shown in Figure 1, the inertia moment of the beam is increased.

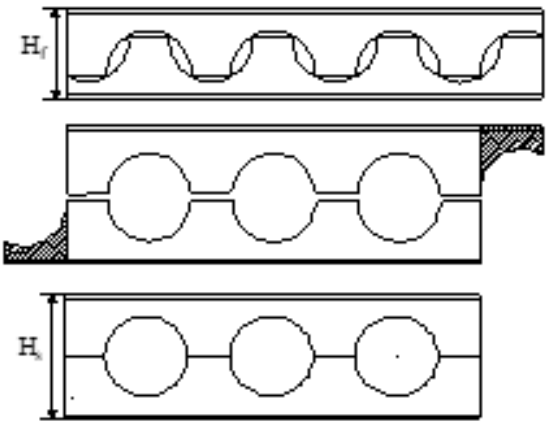

Fig 1. Production stages of cellular beams.

Design methodology

In the design of web expanded cellular steel beams, conducting checks for global bending, shear, secondary (vierendeel) bending is crucial for enhancing the efficiency of these beams.

Global bending capacity: Under non-serviceable loading combinations, the beam should possess sufficient bending capacity to resist external loads. In other words, the maximum moment (*Mu*) under applied load combinations should not exceed the plastic moment capacity (*Mp*) of the beam (Equation 1).

$$M_u = A_{tee} \times p_y \times H_u \leq M_p \quad (1)$$

Where; p_y: Design strength, A_{tee}: Cross-sectional area of T-section, H_u = Distance between the bottom and top T-section centroids.

Shear capacity: Three-stage shear force verification is conducted. Firstly, the shear force check at the supports is performed. The inequality given by Equation (2) ensures that the design shear force value at the supports ($V_{max\ sup}$) does not exceed the beam section's design shear force capacity (P_v).

$$V_{max\ sup} \leq P_v = 0{,}6 \times p_y \times (0{,}9 \times \text{support region cross} - \text{sectional area}) \quad (2)$$

In addition to the initial check, the control of vertical shear force in the beam is carried out with Equation (3). The sum of the shear force capacities at the lower and upper T-sections gives the total shear capacity of the beam. The vertical shear force (V_{Omax}), due to the applied load combination should not exceed the total shear force capacity (P_{vy}).

$$V_{Omax} \leq P_{vy} = 0{,}6 \times p_y \times (0{,}9 \times \sum \text{lower and upper section cross} - \text{sectional area}) \quad (3)$$

Lastly, the lateral shear force verification (Equation 4) is performed. Lateral shear force occurs in the web post of the beam due to axial forces differences in the upper part of the beam (Fig. 2). The lateral force in the web post region of the beam (V_{Hmax}), should be less than the shear force capacity of this region (P_{vh}). In cellular beams, obtaining the internal forces given in Figure 2 is done with Equation (5,6,7).

$$V_{Hmax} \leq P_{vh} = 0{,}6 \times p_y \times (0{,}9 \times \text{minimum cross} - \text{sectional area}) \quad (4)$$

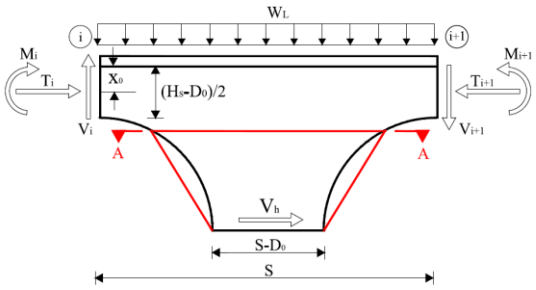

Fig. 2. Lateral shear in the web of the beam.

$V_{i+1} = V_i$
(5)

$M_i = T_i \times (H_s - 2X_0)$
(6)

$V_h = T_{i+1} - T_i = V_{i+1} \frac{S}{H_S - 2X_0}$
(7)

Vierendeel bending capacity: In these beams, the capacity of the lower and upper parts of the beam under bending should be checked (Equation 8). When the beam is subjected to shear, the T-sections at the top and bottom of the beam web should carry the global and secondary moments. The global moment is the classical bending moment on the beam section. The transfer of shear forces through each web causes the secondary (vierendeel) bending moment. Using the Olander[7] approach, the vierendeel bending stresses around the web may be calculated. Olander uses a circular section for the location of the critical section and the ultimate resistance of the T-sections (Figure 3).

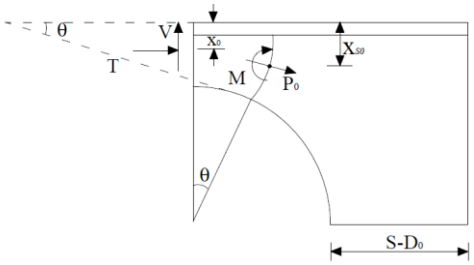

Fig. 3. Olander's curved beam approach.

For symmetric sections, the global shear force is equally distributed between the upper and lower web sections. The interaction between the vierendeel bending moment and axial force at the critical section in the T-section should be checked using Equation (8).

$\frac{P_o}{P_u} + \frac{M}{M_p} \leq 1$
(8)

$P_o = T \cos \emptyset - \frac{V}{2} \sin \emptyset$
(9)

$M = T\,(\chi_{so} - \chi_o) + \frac{V}{2}\,(\frac{H_s}{2} - \chi_{so})$
(10)

Where; P_o= The axial force occurring at the critical section, P_u= Critical section axial force capacity, M=The moment at the critical section, M_p= Critical section moment capacity, T= Axial force occurring in the T-section, V= Shear force occurring in the T-section.

Bending and buckling strength of the web: The buckling and flexural capacity checks of cellular steel beams are performed using Equation (11).

$\frac{M_{allow}}{M_e} = C_1 \left(\frac{S}{D_0}\right) - C_2 \left(\frac{S}{D_0}\right)^2 - C_3 \qquad S - D_0\ [mm]$
(11)

$$C_1 = 5{,}097 + 0.1464\left(\frac{D_0}{t_w}\right) - 0{,}00174\left(\frac{D_0}{t_w}\right)^2 \quad (12)$$

$$C_2 = 1{,}441 + 0.0625\left(\frac{D_0}{t_w}\right) - 0{,}000683\left(\frac{D_0}{t_w}\right)^2 \quad (13)$$

$$C_3 = 3{,}645 + 0{,}0853\left(\frac{D_0}{t_w}\right) - 0.00108\left(\frac{D_0}{t_w}\right)^2 \quad (14)$$

$$M_e = \frac{t_w \times (S - D_0 + 0.564D_0)^2}{6} \times f_y \quad (15)$$

Where; M_{allow}=Allowable maximum web post moment, M_e =Elastic bending moment capacity (Critical sections in Fig. 4), S= Distance between hole centers, t_w =Web post thickness, D_0 =Hole diameter.

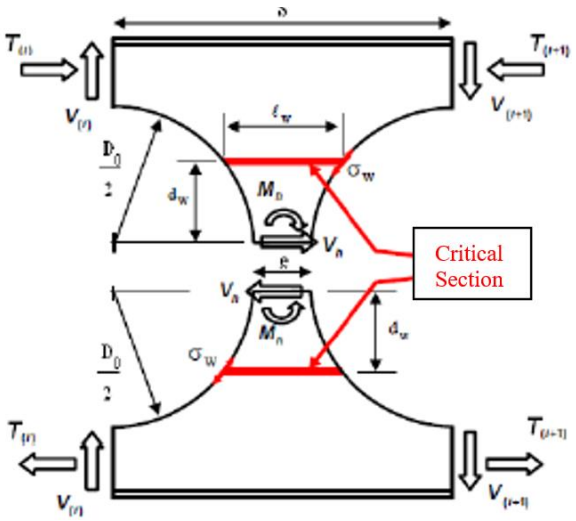

Fig. 4. Web post critical sections.

Test Setup and Equipment

In the experimental phase of the study, the ultimate load-carrying capacities of cellular beams and solid I- beams were tested using a loading frame equipped with a hydraulic power unit. For the measurement of vertical displacements, a displacement transducer (LVDT) was placed in the lower flange at the beam span's L/2 region. Additionally, horizontal displacement transducers were positioned at the beam center for potential lateral displacements. Sliding support was applied at one end, and the other end was supported with a hinge support (Figure 5). The dimensional properties of the beams are detailed in Figure 6

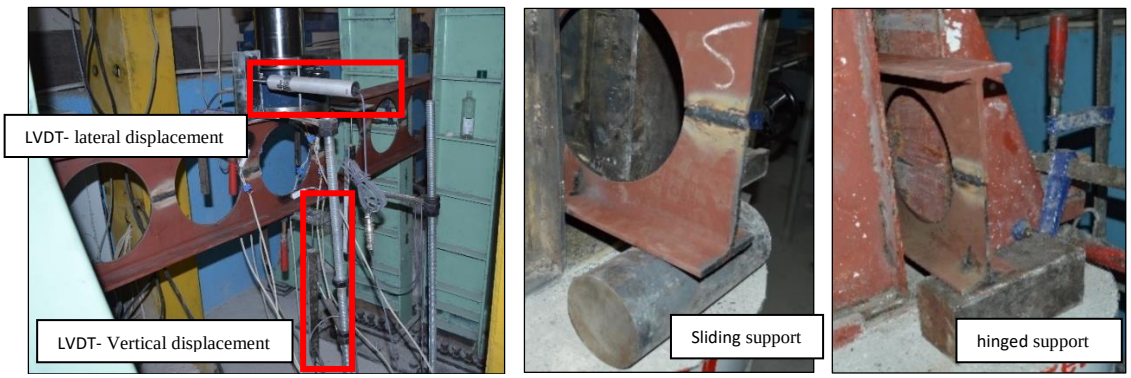

(a) (b) (c)

Fig 5. (a) Placement of LVDT. **(b)** Sliding support. **(c)** hinged support.

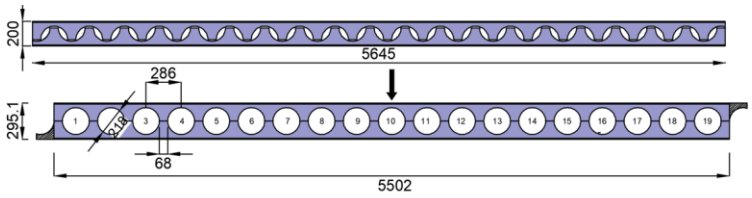

Beam initial height	200 mm	Horizontal Line Length	68 mm
Beam final height	295,1 mm	Number of Holes	19
Hole diameter	218 mm	Beam length	5502 mm
Hole Centers Distance	286 mm		

Fig 6. Dimensional properties of the cellular beam.

In wide spans, especially in the upper flange of the beam, the development of compressive forces can lead to lateral torsional buckling of the section and potential failure of the beam before reaching its load-carrying capacity. To minimize this instability, lateral supports are placed in the L/3 and support regions of the span, as shown in Figure 7. This approach aims to reduce the lateral buckling effects of the beam and enhance its load-carrying capacity. These measures are intended to achieve a safer performance in wide spans by ensuring the durability and structural integrity of the beam.

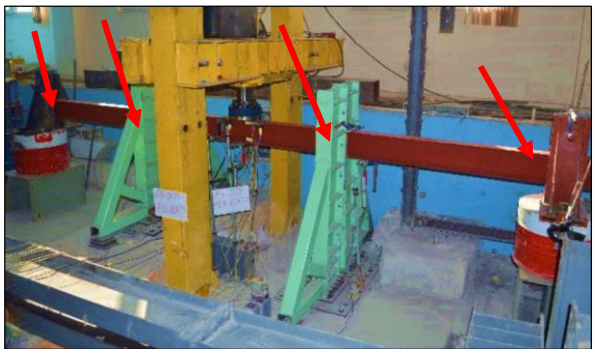

Fig 7. Placement of lateral supports.

III. Results And Discussion

Tests of Web Expanded Cellular Beam

Under a single-point load, tests conducted with IPE_CELL_200 beam models revealed load-carrying capacities of 65,73 kN and 61,93 kN for the beam. The corresponding displacements for these capacities were determined as 47,45 mm and 45,85 mm, respectively. Maximum lateral displacements were determined to be 13 mm and 10,5 mm (Figure 8).

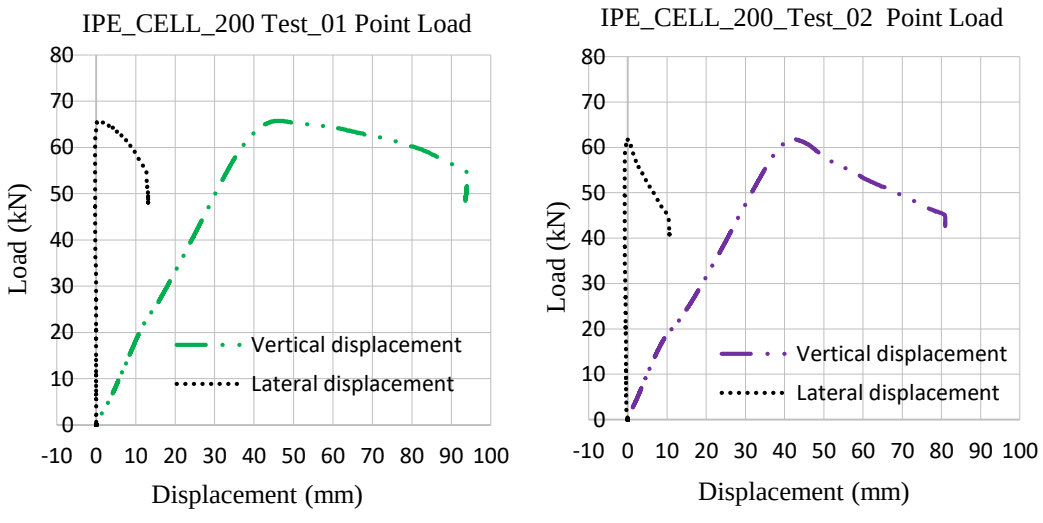

(a) **(b)**

Fig 8. (a) IPE_CELL_200_Test_01. **(b)** IPE_CELL_200_Test_02.

The tests were conducted on IPE_CELL_200 beam models under a single-point load, and according to the obtained results, the average load-carrying capacity is determined to be 63,83 kN, with an average displacement corresponding to maximum loads of 46,65 mm. As shown in Figure 9, especially in the linear region, the beams provided consistent results among themselves, and the graphs overlapped. After reaching the maximum load, a noticeable increase in lateral displacements led to a decrease in load in both experiments.

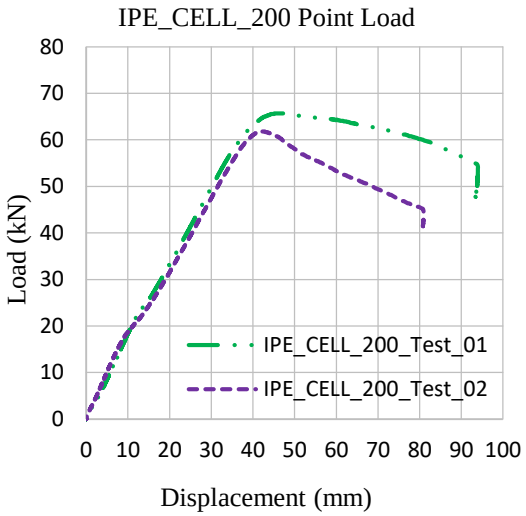

Fig 9. Load-displacement graphs of IPE_CELL_200 beams.

As observed in Figure 10, in both experiments, due to the influence of bending moments, lateral deflection occurred at the center of the beam, accompanied by normal compressive forces at the upper flange. No damage formation was observed in the web post or welds.

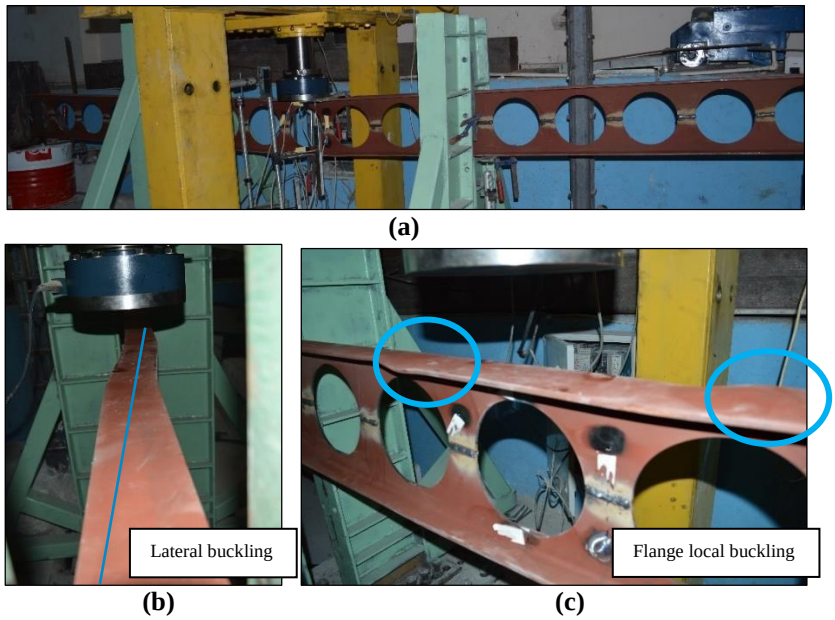

Fig 10. (a) General view. **(b)** Lateral buckling failure mode. **(c)** Flange local buckling failure mode.

Solid I-Beams

According to the results of the test conducted on the IPE_200 beam under a single point load, the load-carrying capacity of the beam was determined as 50,53 kN. The corresponding displacement for this determined capacity was measured as 127.56 mm. Additionally, the maximum lateral displacement was identified as 1 mm. The beam, particularly in the nonlinear region, exhibited stable behavior and continued to displace without a significant decrease in load (Figure 11). During this process, it was observed that the beam underwent plastic

deformation and maintained its ductility characteristics. These results indicate that the beam demonstrated strong performance and durability. The failure mode was observed as flexural bending (Fig. 12).

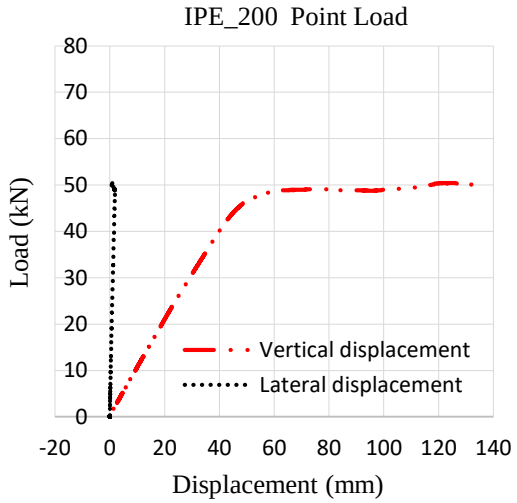

Fig 11. Load-displacement graphs of IPE_200.

Fig 12. Flexural bending failure mode.

IV. Conclusion

This study involved conducting bending tests under a single-point load using IPE200 profiles with a span of 5,5 meters and lateral support. In the test performed with the original IPE_200, the load-carrying capacity of the beam was determined as 50,53 kN and the failure mode was defined as flexural bending. Tests on the IPE_CELL_200 beam model, produced by increasing the web height of the IPE200 profile, showed an average strength of 65,73 kN, with failure modes identified as lateral buckling and flange local buckling. As a result, increasing the web height of the IPE200 profile led to a 30,08% increase in the load-carrying capacity (Table no 1).

Table no 1: Experimental results.

Beam ID	TEST-1 Load (kN)	TEST-1 Displacement (mm)	TEST-2 Load (kN)	TEST-2 Displacement (mm)	Average Displacement (mm)	Average Load (kN)	Load Increase (%)	Failure Mode
IPE_CELL_200	65,73	47,45	61,93	45,85	46,65	63,83	30,08	Lateral buckling Flange local buckling
IPE_200	50,53	127,56	-	-	127,56	50,53		Flexural bending

As can be observed from the load-displacement graphs provided in Figure 13, IPE_CELL_200 beams experienced a significant decrease in load after reaching maximum capacity in the nonlinear region, coinciding with the onset of structural deformations. On the other hand, IPE_200 beams exhibited a more stable behavior than cellular beams in the non-linear region.

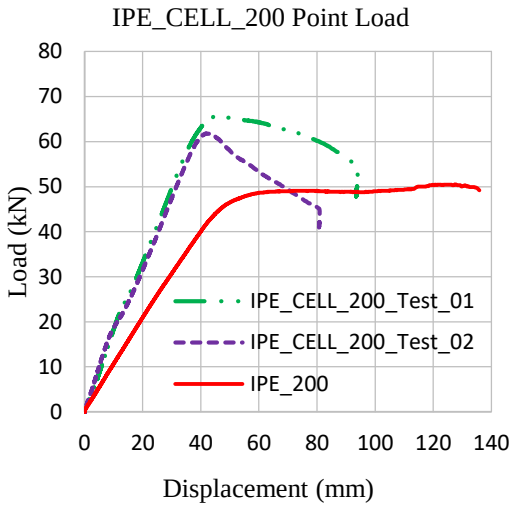

Fig 13. Comparison of load-displacement graphs.

References

[1]. Altifillisch, M.D., Cooke B.R. And Toprac A.A. 1957. An Investigation Of Open Web-Expanded Beams, Welding Research Council Bulletin, 47, 77-88.
[2]. Husain, M.U. And Speirs W.G. 1971. Failure Of Castellated Beams Due To Rupture Of Welded Joints, Acier-Stahl-Steel, 1.
[3]. Sherbourne, A.N. 1966. The Plastic Behavior Of Castellated Beams, Proc. 2nd Commonwealth Welding Conference. Inst. Of Welding, London, Pp:1-5.
[4]. Kerdal, D. And Nethercot, A. 1982. Lateral-Torsional Buckling Of Castellated Steel Beams, Journal Of The Institution Of Structural Engineers, Part A Design And Construction, 60B, 53-61.
[5]. Lawson, R.M. 1985. Design For Openings In Web Of Composite Beams. The Steel Construction Institute.
[6]. Ward, J.K. 1990. Design Of Composite And Non-Composite Cellular Beams, The Steel Construction Institute Publication.
[7]. Olander, H.C. 1953. A Method Of Calculating Stresses In Rigid Frame Corners. Journal Of ASCE.